https://doi.org/10.5194/egusphere-2026-4365
Preprint. Discussion started: 24 July 2026

Delayed State Evolution in Rate-and-State Earthquake Nucleation: Amplification, Localization, and Scaling

Srđan Kostić[1,2] and Nebojša Vasović[3]

[1] Jaroslav Černi Water Institute, Belgrade, Serbia

[2] Faculty of Technical Sciences, University of Novi Sad, Novi Sad, Serbia

[3] University of Belgrade – Faculty of Mining and Geology, Belgrade, Serbia

Correspondence: Srđan Kostić (srdjan.kostic@jcerni.rs)

Email addresses: srdjan.kostic@jcerni.rs (SK); nebojsa.vasovic@rgf.bg.ac.rs (NV)

ORCID: Srđan Kostić – 0000-0002-3705-3080; Nebojša Vasović – 0000-0002-8294-5117

Abstract

Rate-and-state friction assumes instantaneous adaptation of state to slip velocity, but the consequences of this temporal assumption for earthquake nucleation remain poorly constrained. We introduce a constitutive response time t_c into ageing-law feedback and isolate its effect in a spatially distributed fault model. Eight simulations use the same Master configuration and differ only in t_c = 0–0.12 s. Peak velocity increases by approximately 87%, from 7.38×10^{-3} to 1.38×10^{-2} m s^{-1}, while finite delays permit local crossing of 10^{-2} m s^{-1}. The response separates into a moderate-velocity footprint that remains approximately 0.918 km wide and a delay-sensitive high-velocity core that expands to approximately 0.449 km. The response remains localized, separating constitutive amplification from subsequent large-scale propagation. To our knowledge, this is the first spatially distributed demonstration that explicit finite response time in ageing-law feedback can create a high-velocity inner core within a localized nucleation region. The diagnostic $\Pi_d = t_c V_{max}/D_c$ relates delay to state-evolution time. The results establish temporal state adaptation as an independent constitutive dimension and provide benchmarks for laboratory calibration and fully dynamic modelling.

Keywords: rate-and-state friction; friction memory; delayed state evolution; earthquake nucleation; constitutive response time; high-velocity nucleation core

1. Introduction

1.1 Earthquake nucleation as a spatially evolving process

Earthquake nucleation is the progressive localization and acceleration of slip that precedes dynamic rupture. Its evolution is controlled by the competition between frictional weakening, elastic stress redistribution, loading conditions, and the dimensions of velocity-weakening fault regions. Continuum rate-and-state models have shown that nucleation is not adequately described by a single point or onset time: the size, shape, and internal velocity distribution of the slipping region evolve before rapid rupture begins (Rice, 1993; Rubin and Ampuero, 2005; Ampuero and Rubin, 2008). Accordingly, a constitutive mechanism can influence nucleation even when it does not immediately produce large-scale propagation.

Classical rate-and-state friction provides the principal framework for describing this process. The formulation introduced by Dieterich (1979) and Ruina (1983) combines a direct dependence on slip velocity with an internal state variable representing the evolving condition of frictional contacts. Laboratory observations and contact-scale interpretations support the importance of time-dependent healing and contact renewal (Dieterich and Kilgore, 1994; Marone, 1998). When coupled to an elastic fault, the law reproduces stable sliding, accelerating nucleation, seismic cycles, and spontaneous rupture episodes across a broad range of models (Lapusta et al., 2000; Kaneko et al., 2008).

A major focus of previous research has been the choice of state-evolution law. Rubin and Ampuero (2005) and Ampuero and Rubin (2008) showed that ageing and slip laws can produce different nucleation styles and characteristic lengths. Kame et al. (2015) examined a revised rate-and-state law, while Viesca (2023) demonstrated that the nonlinear nucleation length depends fundamentally on how frictional state evolution is formulated. Microphysical and multi-mechanism approaches have further related state-dependent friction to gouge deformation, contact processes, temperature, and competing healing mechanisms (Ikari et al., 2016; van den Ende et al., 2018; Barbot, 2022). These

https://doi.org/10.5194/egusphere-2026-4365
Preprint. Discussion started: 24 July 2026

studies establish that the constitutive description of state matters, but they generally retain an instantaneous relationship between the current mechanical state and the state evolution rate.

1.2 Instantaneous state adaptation as an unresolved constitutive assumption

In the classical ageing law, the state derivative at time t is calculated from velocity and state at that same time. The state variable stores the accumulated condition of the interface, but the update rule itself has no independent response time. This convention implicitly assumes that contact renewal, healing, and gouge reorganization adapt immediately to a velocity change. Such an approximation is convenient and often appropriate, yet it is not equivalent to demonstrating that the physical processes represented by state are instantaneous.

Earlier phenomenological earthquake models introduced explicit delay as a representation of frictional memory. Kostić et al. (2013a, 2013b) showed that delay and friction strength can alter oscillatory, quasiperiodic, creeping, and arrested behavior in one- and two-block Burridge–Knopoff-type systems. Vasović et al. (2016) further examined interaction delays in a stochastic fault model. These studies established that temporal memory can be dynamically consequential. Their low-dimensional structure, however, cannot resolve how an explicit local constitutive response time changes the velocity distribution within a finite nucleation region.

This limitation defines the gap addressed here. Continuum rate-and-state studies resolve the spatial structure of nucleation but normally use instantaneous state adaptation; delayed block models resolve temporal memory but do not resolve an evolving nucleation field. Connecting these two lines of research requires a controlled spatial model in which the standard friction parameters, stress state, geometry, and nucleation perturbation remain fixed while only the response time of the state feedback is varied. Such a comparison can determine whether delay merely retimes nucleation or changes its amplitude and internal spatial organization.

The distinction is conceptually important. Constitutive modelling involves both the physical content of a friction law and the temporal architecture through which that content responds to transient loading. Two laws may contain similar state variables but adapt on different timescales; conversely, the same steady-state friction relation may produce different transient behavior when state adaptation is delayed. Constitutive response time should therefore be tested as a modelling dimension in its own right, rather than treated solely as a numerical detail.

1.3 Research gap, novelty, and objectives

The central research question is: does a finite constitutive response time modify the amplitude, temporal evolution, and internal spatial organization of earthquake nucleation independently of the conventional rate-and-state parameters? A related question is whether delayed state evolution can create a localized high-velocity core before the surrounding fault is recruited into larger-scale propagation. These questions are narrower than asking whether delay alone produces an unrestricted dynamic earthquake, but they address the constitutive stage at which such a transition may be prepared.

To answer them, we introduce a delayed ageing-law feedback into a one-dimensional spatially distributed fault model. Eight simulations use the same documented Master configuration and differ only in t_c. We evaluate the full space–time velocity field, profiles at common times, center-point histories, peak velocity, spatial extents above 10^{-3} and 10^{-2} m s^{-1}, an integrated moment proxy, and a localization criterion. This multi-observable design distinguishes a simple change in peak amplitude from a reorganization of the nucleation field.

The anticipated scientific contribution is threefold. First, to our knowledge, the study provides the first spatially distributed test of an explicit finite response time in local ageing-law feedback under otherwise identical rate-and-state conditions. Second, it evaluates whether moderate- and high-velocity parts of the nucleation zone have different sensitivities to constitutive memory. Third, it introduces the diagnostic $\Pi_d = t_c V_{max}/D_c$ to relate the delay to the characteristic state-evolution time. The aim is not to prescribe a universal natural-fault value of t_c, but to establish a reproducible mechanistic and numerical basis for its subsequent laboratory calibration and implementation in fully dynamic rupture models.

2. Constitutive framework and numerical methodology

2.1 Classical rate-and-state reference formulation

The reference friction coefficient follows the logarithmic rate-and-state form of Dieterich (1979) and Ruina (1983):

2

https://doi.org/10.5194/egusphere-2026-4365
Preprint. Discussion started: 24 July 2026

$$f(x,t) = f_0 + a(x) \ln[V(x,t)/V_0] + b(x) \ln[\theta(x,t)V_0/D_c]. \quad (1)$$

Here f_0 is the reference coefficient at velocity V_0, a and b are the direct- and state-effect parameters, θ is the state variable, and D_c is the characteristic slip distance. Frictional shear resistance is

$$\tau_f(x,t) = \sigma_{eff} f(x,t), \quad (2)$$

where σ_{eff} is the effective normal stress. In the velocity-weakening region b > a, whereas the surrounding margins satisfy a > b. Smooth transitions avoid discontinuities in the constitutive parameters. The instantaneous reference case uses the classical ageing law

$$d\theta(x,t)/dt = 1 - V(x,t)\theta(x,t)/D_c. \quad (3)$$

Equation (3) represents time-dependent contact ageing through the unit healing term and state consumption through accumulated sliding. It is recovered exactly in the present formulation when $t_c = 0$.

2.2 Delayed state-evolution formulation

Frictional memory is introduced by evaluating the velocity–state feedback at the retarded time $t - t_c$ while retaining Eq. (1) for the current frictional resistance:

$$d\theta(x,t)/dt = 1 - V(x,t - t_c)\theta(x,t - t_c)/D_c. \quad (4)$$

The new parameter t_c is a constitutive response time. It does not change the prescribed steady-state friction curve, a, b, D_c, or the direct velocity effect. Instead, it controls how rapidly the ageing-law feedback adapts during transient acceleration. The tested values are t_c = 0, 0.002, 0.005, 0.01, 0.02, 0.04, 0.08, and 0.12 s. This range was selected to resolve the initial threshold crossing and its subsequent growth within the 12 s analysis window; it is a controlled numerical range rather than a calibrated natural-fault interval.

For $t < t_c$, the delayed variables are supplied by the common initial history. During integration, velocity and state histories are retained in a discrete circular buffer and values at $t - t_c$ are evaluated by linear interpolation. The same algorithm is used for all cases, with Eq. (3) obtained at zero lag. This implementation prevents the delay comparison from being confounded by different time integrators or initial histories.

2.3 Spatially distributed fault model

The constitutive law is coupled to a one-dimensional distributed fault model with inertia, nearest-neighbour elastic wave coupling, and radiation damping. Displacement u(x,t) and slip velocity V(x,t) satisfy

$$\partial u/\partial t = V, \quad (5)$$

$$\partial V/\partial t = c_s^2\, \partial^2 u/\partial x^2 + \{\tau_{load}(x) - \tau_f(x,t) - \eta[V - V_{init}]\}/(\rho H). \quad (6)$$

Here ρ and c_s are density and shear-wave speed, H is the effective thickness of the reduced-order representation, and $\eta = \rho\, c_s/2$ is the radiation-damping coefficient. The choice $H = \Delta x$ is an explicit numerical closure. Equation (6) resolves distributed inertial and elastic interaction along the fault, but it is not a spectral boundary-integral representation of an unrestricted two-dimensional rupture. Its purpose is to isolate the spatial signature of the delayed constitutive term efficiently and reproducibly.

The 40 km periodic domain contains a 24 km velocity-weakening region, 0.5 km smooth transitions, and two 8 km velocity-strengthening margins. A smooth cosine stress perturbation with radius R_{nuc} = 1 km and maximum amplitude $\Delta\tau_{max}$ = 2 MPa initiates slip at the domain center. The initial shear traction is τ_0 = 6 MPa and effective normal stress is 10 MPa. The state field is calculated from frictional consistency, $\tau_f(V_{init},\theta_0) = \tau_0$, so that every simulation begins from the same constitutive equilibrium rather than from the approximation $\theta_0 = D_c/V_0$.

2.4 Numerical design and response measures

The domain is discretized using N = 2048 nodes, giving Δx = 19.53125 m. The final calculations use $\Delta t = 2.5 \times 10^{-4}$ s, refined from the 10^{-3} s pilot value, and extend to T_{max} = 12 s. The Courant ratio $c_s\Delta t/\Delta x$ is approximately 0.044, well below the implemented stability gate. Periodic boundaries are sufficiently distant from the localized response that no boundary interaction enters the analyzed region. Table S1 in the Supplement summarizes all adopted, derived, and closure parameters; the same values are also printed within Figures 1–7.

https://doi.org/10.5194/egusphere-2026-4365
Preprint. Discussion started: 24 July 2026

The primary amplitude measure is $V_{max} = max_{x,t}V(x,t)$. Spatial organization is quantified by L_q, the total grid length for which $max_t\ V(x,t) \geq q$, using $q = 10^{-3}$ and 10^{-2} m s^{-1}. The lower level tracks the moderate-velocity nucleation footprint, while the higher level identifies the rapidly slipping core. Center-point histories and profiles at 3, 6, 9, and 12 s resolve temporal and spatial changes that cannot be represented by a single peak value. The final moment proxy is the spatial integral of displacement, $\int u(x,T_{max})dx$; it is used comparatively and is not converted to seismic moment because the reduced model does not prescribe a physical along-strike area.

A local velocity-threshold crossing is recorded when $V_{max} \geq 10^{-2}$ m s^{-1}. Spatial propagation beyond the prescribed nucleation scale is evaluated separately: a case would be classified as distributed dynamic propagation only if the region exceeding 10^{-2} m s^{-1} became wider than the 2 km nucleation zone. Separating these criteria avoids equating a local high velocity with earthquake-scale rupture propagation. Finally, the dimensionless diagnostic

$$\Pi_d = t_c\, V_{max}/D_c \qquad (7)$$

compares the response delay with the realized state-evolution time D_c/V_{max}. Because it contains an output quantity, Π_d is used to organize the computed responses rather than as an a priori predictor.

3. Results

The numerical experiments were designed as a controlled constitutive comparison. All eight simulations use the same Master geometry, stress state, friction parameters, nucleation perturbation, grid, time step, and reduced-order elastic closure; only the constitutive response time t_c is varied. The results are therefore interpreted through seven complementary visualizations. Figures 3 and 5–7 resolve the space–time structure of nucleation, Figure 2 quantifies its integral measures, Figure 6 introduces a dimensionless organization, and Figure 7 separates the onset of locally rapid slip from spatial recruitment beyond the nucleation zone. This sequence makes it possible to test whether delayed state evolution changes only the timing of the response or changes the nucleation process itself.

3.1 Delayed-state amplification of localized nucleation

Figure 1 provides the first direct space–time comparison of the instantaneous reference and three representative delayed-state cases. In every panel, acceleration begins at the center of the imposed perturbation and remains symmetric about x = 0, confirming that differences between the simulations are not caused by a shift in nucleation position or by boundary interaction. The dashed lines at x = ±1 km delimit the initially stressed nucleation region, while the velocity contours distinguish moderate acceleration ($V = 10^{-3}$ m s^{-1}) from the faster inner response ($V = 10^{-2}$ m s^{-1}).

For $t_c = 0$, the accelerated region develops gradually but remains below the higher threshold throughout the 12 s interval. Introducing a response time of only 0.01 s changes this behavior: a narrow high-velocity core appears near the end of the simulation. At $t_c = 0.04$ s the core is more persistent and spatially wider, and at $t_c = 0.12$ s it becomes the dominant feature of the central response. The systematic progression across panels demonstrates that delayed state evolution amplifies the same nucleation episode rather than generating a separate nucleation site.

The novelty of Figure 1 lies in its spatially resolved representation of explicit local frictional delay. Earlier delayed Burridge–Knopoff-type studies identified changes in temporal regimes of one- and two-block systems, but could not show how delay restructures velocity inside a finite nucleation zone. To our knowledge, Figure 1 is the first spatially distributed demonstration, within a controlled rate-and-state nucleation model, that a finite ageing-law response time can generate a high-velocity inner core while the broader nucleation footprint remains localized.

https://doi.org/10.5194/egusphere-2026-4365
Preprint. Discussion started: 24 July 2026

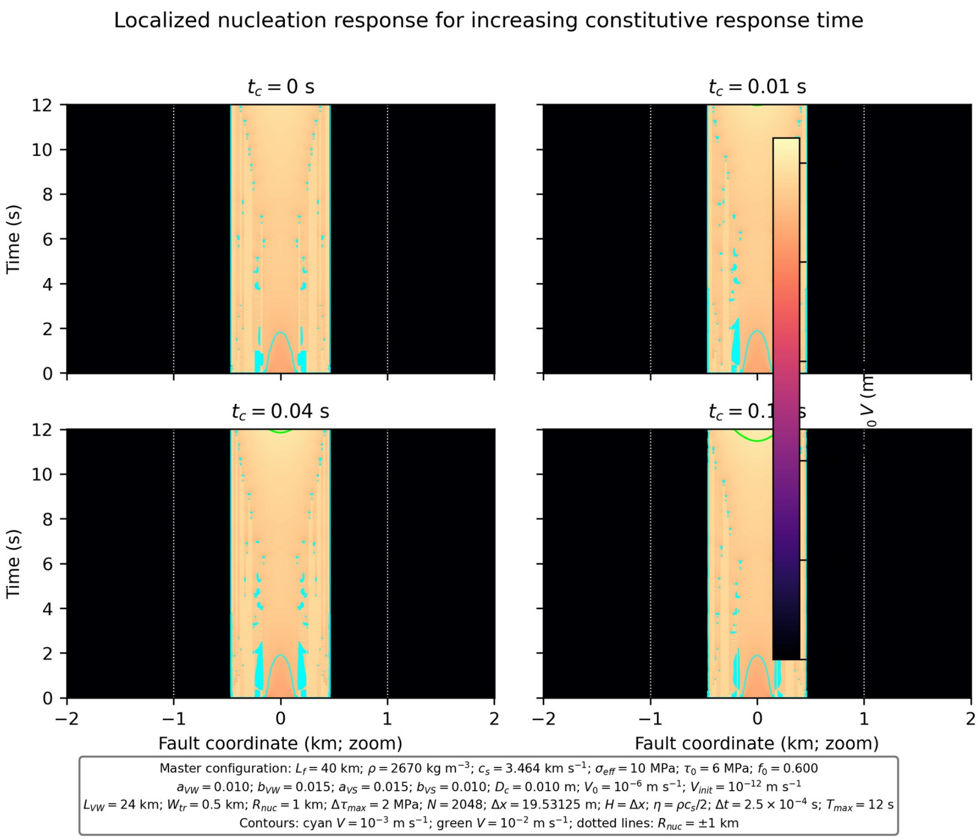

Figure 1. Space–time evolution of localized slip velocity for t_c = 0, 0.01, 0.04, and 0.12 s. Dashed lines mark the ±1 km nucleation boundary; contours denote V = 10^{-3} and 10^{-2} m s^{-1}. Parameter values used for the calculation are printed on the figure.

3.2 Systematic dependence on constitutive response time

Figure 2 quantifies the trends suggested by the space–time fields. Peak velocity increases from 7.38 × 10^{-3} m s^{-1} in the instantaneous case to 1.02 × 10^{-2} m s^{-1} already at t_c = 0.002 s. The response remains close to the threshold for t_c = 0 .005–0.02 s and then strengthens more rapidly, reaching 1.08 × 10^{-2}, 1.22 × 10^{-2}, and 1.38 × 10^{-2} m s^{-1} at t_c = 0.04, 0.08, and 0.12 s, respectively. The end-member increase is approximately 87%. The very short delay required to cross the adopted velocity threshold shows that the instantaneous model is close to a constitutive transition that is not visible when t_c is fixed at zero.

The two spatial measures behave differently. The width above 10^{-3} m s^{-1} remains 0.918 km for all simulations, whereas the width above 10^{-2} m s^{-1} changes from zero at t_c = 0 to 0.098 km at 0.002 s and expands to 0.449 km at 0.12 s. Its detailed variation at short delays is not strictly monotonic, but the long-delay trend is unequivocal. The moment proxy initially decreases slightly, from 42.54 to approximately 41.18–41.49, before rising to 42.84 and 43.91 for the two largest response times. This non-monotonic integral behavior is important: constitutive memory first redistributes slip toward a faster central core and only at larger t_c produces a net increase in the integrated response.

In contrast to previous delay studies that primarily classified periodic, quasiperiodic, creeping, or arrested block motion, Figure 2 quantifies how explicit response time partitions a spatial nucleation event into amplitude, footprint, high-velocity extent, and integrated-slip effects. The combined metrics provide evidence that t_c is an independent constitutive control parameter. Its influence cannot be represented by reporting only a later onset time or a single peak value.

https://doi.org/10.5194/egusphere-2026-4365
Preprint. Discussion started: 24 July 2026

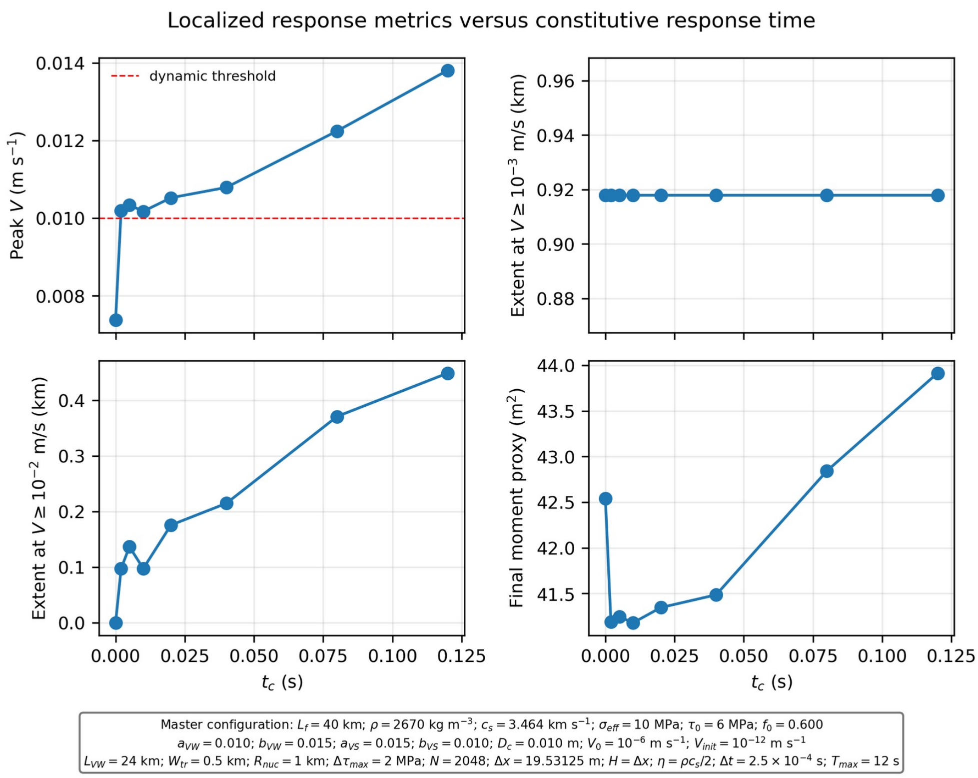

Figure 2. Peak velocity, spatial extents above 10^{-3} and 10^{-2} m s^{-1}, and moment proxy as functions of t_c. Symbols correspond to the eight simulations. Master parameters are shown in the embedded annotation.

https://doi.org/10.5194/egusphere-2026-4365
Preprint. Discussion started: 24 July 2026

3.3 Spatial and temporal reorganization

Figure 3 compares full velocity profiles at 3, 6, 9, and 12 s. At 3 s the profiles are nearly coincident, indicating that the imposed perturbation and early elastic response dominate before sufficient delayed feedback has accumulated. Differences become visible at 6 s and strengthen at 9 s. By 12 s, the delayed cases display a progressively higher and sharper maximum at x = 0, while velocities outside the central kilometre remain close to the instantaneous solution. The response-time effect is therefore spatially selective rather than a uniform multiplicative scaling of the entire velocity field.

The evolution of the profile shoulders is especially informative. Their limited outward movement explains why the 10^{-3} m s^{-1} footprint is nearly invariant, whereas the growing central curvature and peak explain the expansion of the 10^{-2} m s^{-1} core. Figure 3 thus provides the spatial mechanism behind the two-scale behavior measured in Figure 2. To our knowledge, this profile-level separation between a perturbation-controlled outer scale and a memory-controlled inner scale has not previously been reported for an explicit delayed ageing law.

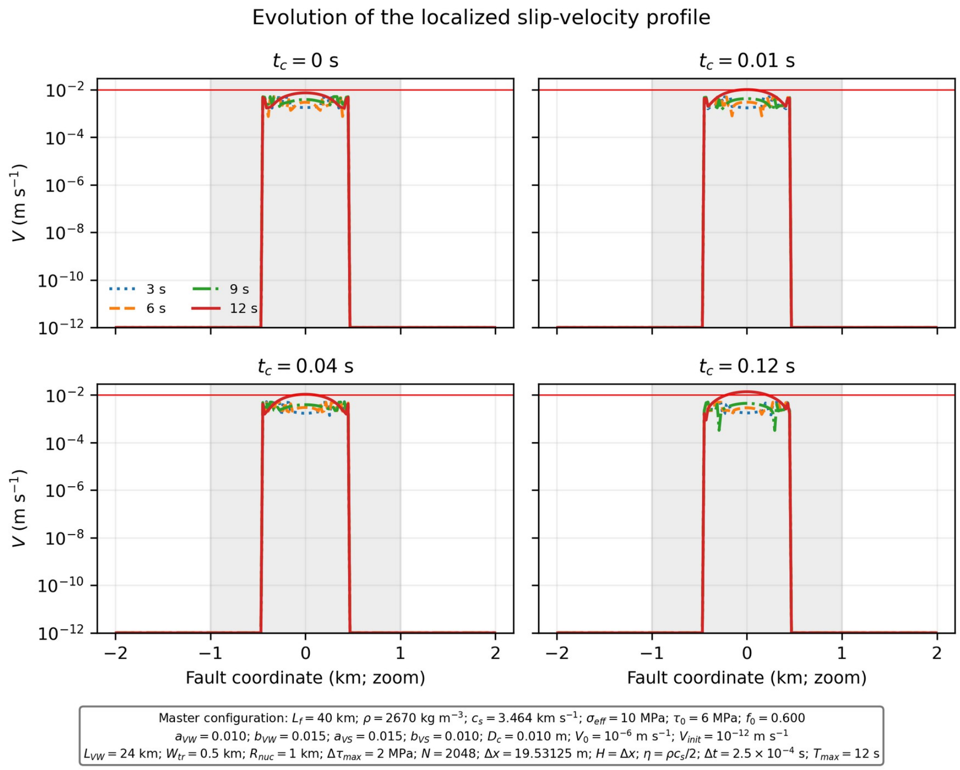

Figure 3. Slip-velocity profiles at 3, 6, 9, and 12 s for representative constitutive response times. The comparison isolates the delay-induced spatial reorganization within the nucleation region. Parameters are listed on the figure.

Figure 4 isolates the center point, where the constitutive memory effect is strongest. All curves begin from the same initial condition and follow a common early trajectory, after which they separate progressively. The separation is ordered most clearly for the longer delays: $t_c = 0.08$ and 0.12 s produce the strongest late-time acceleration, whereas the instantaneous solution remains the lowest. The absence of an abrupt imposed change in loading confirms that the divergence is generated internally by the delayed state feedback.

Read together, Figures 5 and 6 show that frictional delay modifies both space and time. The center histories establish amplitude and temporal divergence, while the profiles show that this divergence is concentrated in the inner nucleation zone. This combined spatial–temporal evidence is stronger than the trajectory comparisons available from earlier low-dimensional delayed models and is central to the present paper's advance from block dynamics to distributed nucleation.

https://doi.org/10.5194/egusphere-2026-4365
Preprint. Discussion started: 24 July 2026

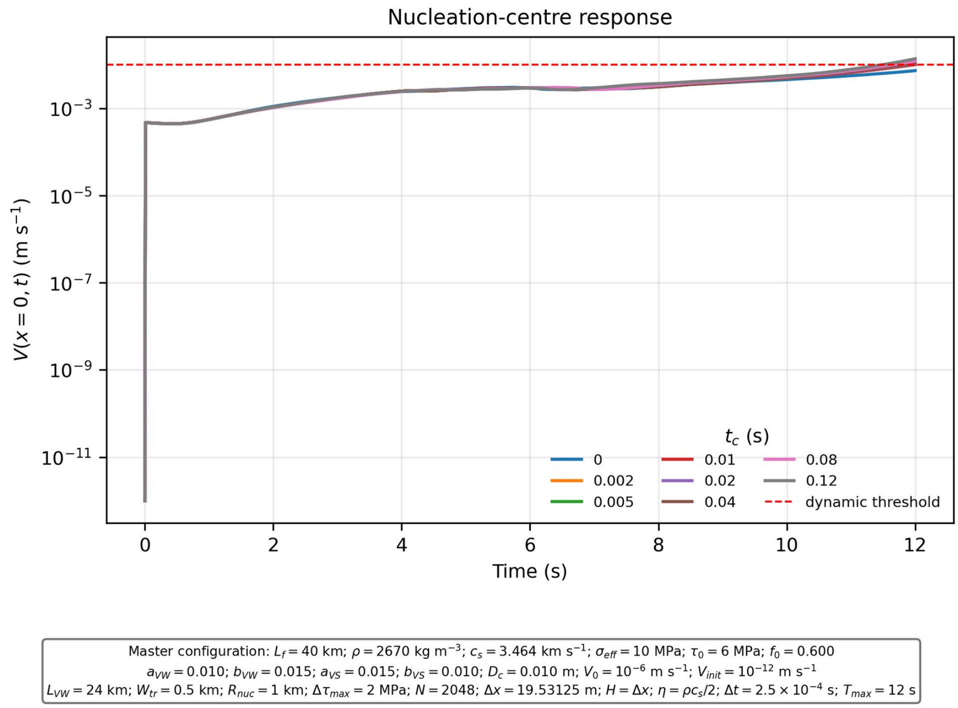

Figure 4. Slip-velocity histories at the center of the nucleation zone for all tested values of t_c. Finite response time progressively increases and retimes the acceleration. Parameters are listed on the figure.

https://doi.org/10.5194/egusphere-2026-4365
Preprint. Discussion started: 24 July 2026

3.4 Memory-strength scaling and regime identification

Figure 5 condenses each simulation into the maximum velocity attained at every position and arranges the results as a function of t_c. The map reveals a persistent central band associated with the imposed perturbation and a brighter inner zone that develops as delay increases. The 10^{-3} m s^{-1} boundary is nearly vertical across the parameter range, whereas the 10^{-2} m s^{-1} contour is absent at $t_c = 0$ and progressively encloses a wider region at larger delays. This geometry visually confirms that the outer and inner scales respond to different controls.

The map also demonstrates continuity rather than a collection of unrelated numerical cases. No secondary high-velocity patches appear, and the maximum always remains at $x = 0$. The response evolves from an instantaneous-state nucleation profile toward a delay-amplified profile through a coherent deformation of the same spatial structure. Figure 5 is therefore a regime map of constitutive memory within the nucleation zone. Compared with earlier work on instantaneous state evolution, the new axis is not a conventional friction coefficient or patch dimension but the finite time required for state feedback to adapt.

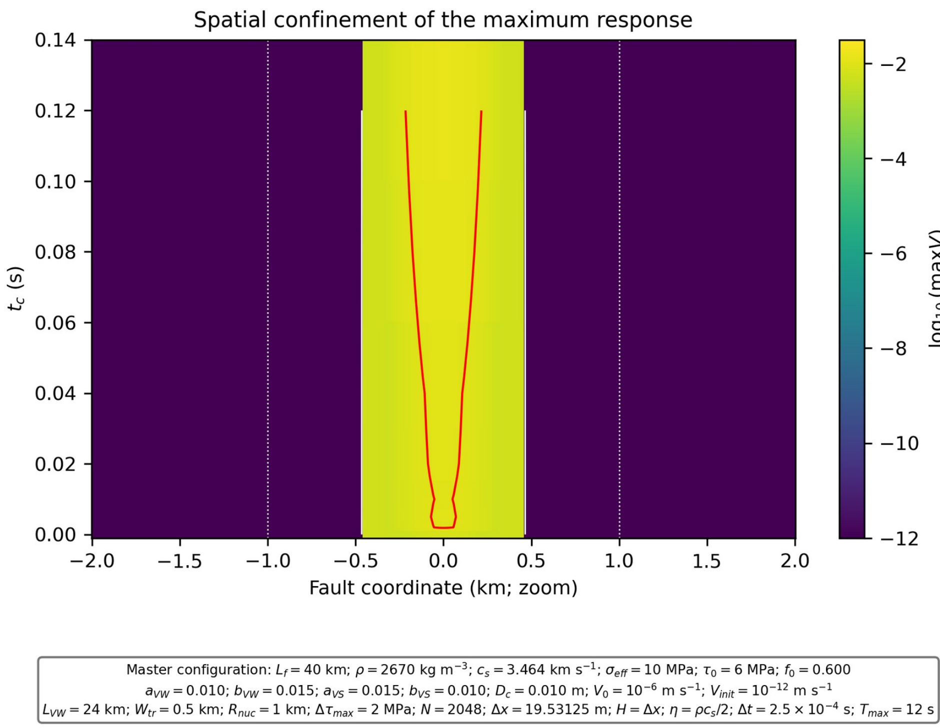

Figure 5. Maximum slip velocity attained at each position as a function of t_c. The map shows amplification and widening of the high-velocity nucleation core. Parameters are listed on the figure.

Figure 6 reorganizes the results using $\Pi_d = t_c V_{max}/D_c$, which compares the imposed response delay with the characteristic state-evolution time D_c/V_{max}. The instantaneous case occupies $\Pi_d = 0$, while increasing response time moves the simulations toward larger memory strength. Normalized peak velocity rises with Π_d, and the high-velocity extent follows the same overall progression. The common trend indicates that the observed effects depend on the amount of characteristic slip that can occur before the delayed state feedback has adapted.

The introduction of Π_d is a second novelty of the Results. Earlier delayed block models used delay as an external bifurcation parameter, whereas Figure 6 relates that delay directly to the established rate-and-state length D_c and the realized nucleation velocity. Π_d is not yet a predictive input parameter because it contains V_{max}, but it supplies an objective post-simulation measure for comparing memory strength and provides a target for the input-based scaling proposed in the Conclusions.

https://doi.org/10.5194/egusphere-2026-4365
Preprint. Discussion started: 24 July 2026

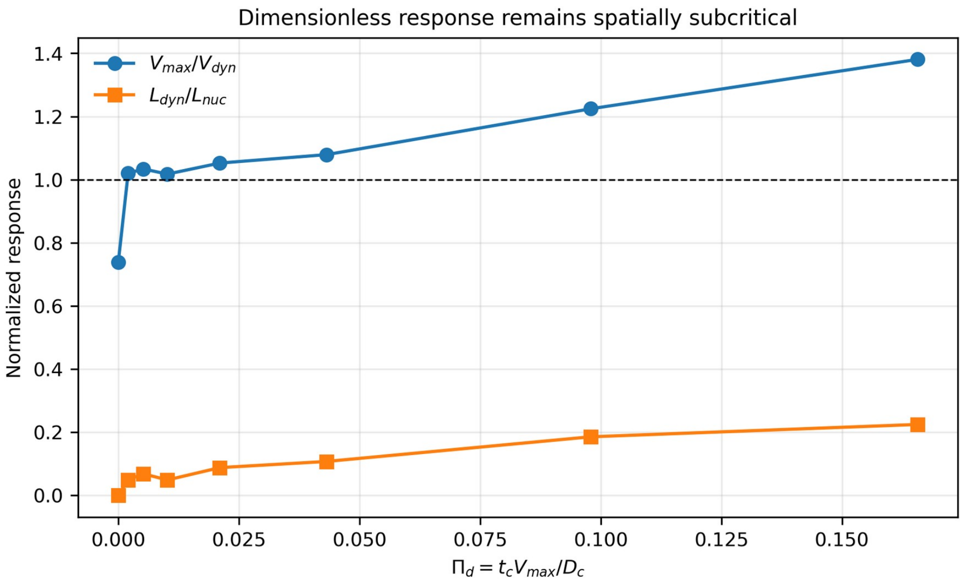

Master configuration: $L_f = 40$ km; $\rho = 2670$ kg m^{-3}; $c_s = 3.464$ km s^{-1}; $\sigma_{eff} = 10$ MPa; $\tau_0 = 6$ MPa; $f_0 = 0.600$
$a_{VW} = 0.010$; $b_{VW} = 0.015$; $a_{VS} = 0.015$; $b_{VS} = 0.010$; $D_c = 0.010$ m; $V_0 = 10^{-6}$ m s^{-1}; $V_{init} = 10^{-12}$ m s^{-1}
$L_{VW} = 24$ km; $W_{tr} = 0.5$ km; $R_{nuc} = 1$ km; $\Delta\tau_{max} = 2$ MPa; $N = 2048$; $\Delta x = 19.53125$ m; $H = \Delta x$; $\eta = \rho c_s/2$; $\Delta t = 2.5 \times 10^{-4}$ s; $T_{max} = 12$ s

Figure 6. Response metrics organized by the dimensionless memory strength $\Pi_d = t_c V_{max}/D_c$. The normalized peak and dynamic-threshold extent both increase as memory becomes stronger. Parameters are listed on the figure.

10

https://doi.org/10.5194/egusphere-2026-4365
Preprint. Discussion started: 24 July 2026

Figure 7 places the two diagnostic criteria side by side. The red curve shows that the peak velocity crosses 10^{-2} m s^{-1} as soon as a finite response time is introduced and then rises further for the largest t_c values. The shaded spatial measure remains confined to a fraction of the 2 km nucleation width, and the maximum outside the nucleation zone remains at the locked-background level. The figure therefore separates the attainment of locally rapid slip from the subsequent recruitment of the surrounding fault.

This distinction strengthens the interpretation of the preceding figures. A classification based only on V_{max} would identify a transition to locally dynamic velocity, whereas a classification based only on propagation would overlook the substantial constitutive amplification occurring before outward growth. The results establish an intermediate, spatially localized high-velocity nucleation regime controlled by t_c. To our knowledge, this regime has not previously been isolated using an explicit local delayed ageing law in a spatially distributed fault model.

Relative to the earlier delayed block studies, the advance is the ability to distinguish amplitude transition from spatial propagation. Relative to classical continuum RSF nucleation studies, the advance is the demonstration that finite constitutive adaptation—without changing a, b, D_c, stress, or patch geometry—can move the system across a velocity threshold and create a wider high-velocity core. Figures 1–7 collectively support the paper's principal novelty claim: temporal organization of state evolution is an independent and spatially observable dimension of earthquake nucleation.

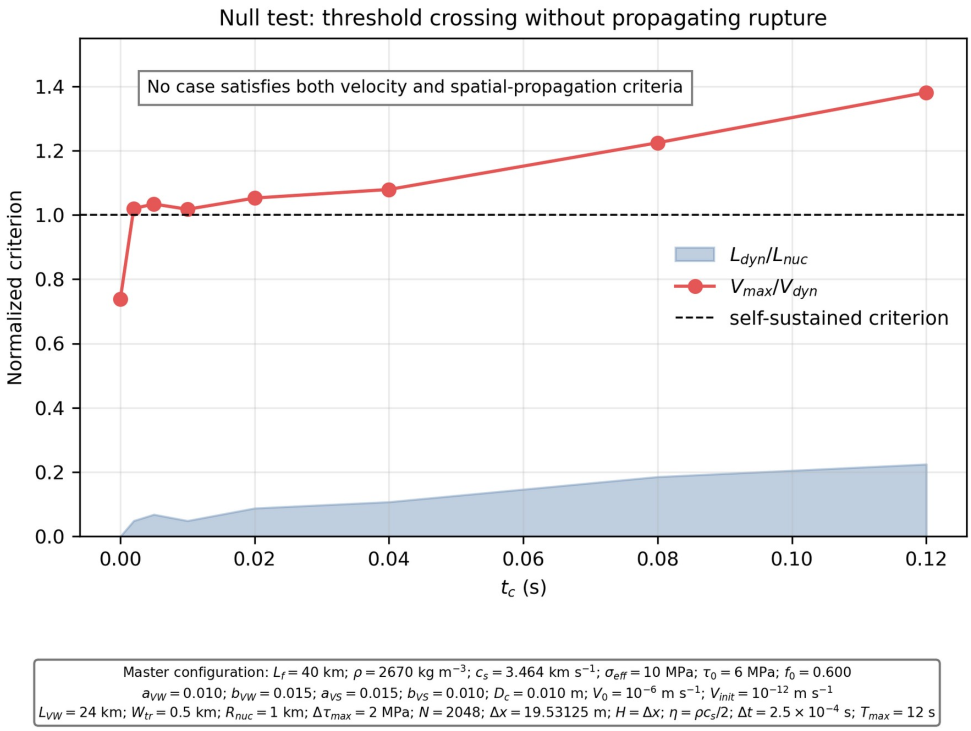

Figure 7. Classification of the delayed-state response using the adopted velocity threshold and spatial localization criterion. Constitutive delay produces locally dynamic slip speeds while retaining a nucleation-scale footprint. Parameters and threshold definitions are printed on the figure.

4. Discussion

The results demonstrate that constitutive response time is an independent control on earthquake nucleation, rather than a minor numerical correction to the classical rate-and-state formulation. When all elastic, frictional, geometrical, loading, and nucleation parameters are held fixed, varying only t_c systematically changes the maximum slip velocity, the timing of acceleration, and the spatial distribution of accelerated slip. Across the investigated interval, V_{max} increases by approximately 87%, from 7.38×10^{-3} to 1.38×10^{-2} m s^{-1}. The response therefore cannot be reproduced

https://doi.org/10.5194/egusphere-2026-4365
Preprint. Discussion started: 24 July 2026

simply by shifting the origin of time: the delayed solutions acquire a different amplitude and a different internal spatial structure. This is the central physical result of the study. Frictional memory changes how instability develops inside the nucleation zone even when the conventional rate-and-state parameters a, b, D_c, f_0, and V_0 are unchanged.

This finding extends the classical rate-and-state framework established by Dieterich (1979) and Ruina (1983). In that framework, the state variable represents the evolving maturity and real contact population of the slipping interface, consistent with the contact-scale interpretation developed by Dieterich and Kilgore (1994) and reviewed by Marone (1998). The ageing law assumes that the state derivative responds to the instantaneous values of velocity and state. Consequently, memory is present through the value of θ itself, but the constitutive update has no additional finite response time. Our formulation retains the familiar logarithmic rate-and-state friction coefficient and changes only the temporal organization of state evolution by evaluating the ageing feedback at $t - t_c$. The comparison with $t_c = 0$ is therefore unusually controlled: it does not compare different friction laws or different parameter calibrations, but isolates the effect of a finite adaptation time within the same constitutive structure.

Previous continuum studies have shown that earthquake nucleation is highly sensitive to the selected state-evolution law. Rubin and Ampuero (2005) derived nucleation behavior for ageing rate-and-state faults, while Ampuero and Rubin (2008) demonstrated important differences between ageing and slip laws in two-dimensional quasi-static nucleation. Kame et al. (2015) and Viesca (2023) further showed that revisions to state evolution can alter the characteristic nucleation process and even the theoretical status of a unique nucleation length. These studies establish that the mathematical form of state evolution matters. The present work addresses a different and complementary question: what changes when the form and calibrated parameters are retained, but the state response is no longer instantaneous? Figures 1–7 show that this temporal change alone is sufficient to produce a measurable and systematic modification of nucleation. Thus, the relevant constitutive choice is not limited to which state law is used; it also includes how rapidly that law is allowed to respond to an evolving slip rate.

The study also differs from fully dynamic rate-and-state simulations such as those of Lapusta et al. (2000) and Kaneko et al. (2008). Those models resolve spontaneous earthquake sequences or dynamic rupture with instantaneous state evolution and have clarified the roles of elastic interactions, velocity-strengthening regions, and wave-mediated stress transfer. They provide the appropriate benchmark for future large-scale implementation of the delayed law. The purpose of the present reduced-order distributed model is more specific: to separate the local constitutive memory effect from the many mechanisms that control unrestricted rupture propagation. This separation makes the causal interpretation of Figures 1–7 stronger. Because the Master configuration, perturbation, discretization, and elastic closure are identical in all simulations, the observed amplification and spatial reorganization can be attributed directly to t_c. At the same time, the localized response should not be interpreted as a substitute for a fully dynamic boundary-integral or finite-element calculation of earthquake-scale rupture length and speed.

The closest conceptual predecessors are the delayed earthquake models of Kostić et al. (2013a, 2013b). Those studies introduced explicit time delay into low-dimensional Burridge–Knopoff-type systems and showed that delay and friction strength can generate transitions among oscillatory, quasiperiodic, creeping, and arrested regimes. They established the broader proposition that fault friction may retain a finite memory of its sliding history. However, one- and two-block systems cannot determine how this memory is expressed spatially inside a nucleation zone. They do not resolve the width of the accelerated region, the coexistence of moderate- and high-velocity slip domains, or the way in which a local velocity threshold is reached at different positions. The present study advances that earlier idea from temporal regime changes in a few degrees of freedom to spatially distributed nucleation. This step is scientifically important because earthquake initiation is not defined only by the motion of a representative block; it is an evolving localization process governed by the interaction between constitutive weakening and elastic coupling.

The most distinctive result is the emergence of two spatial response scales. The width over which V exceeds 10^{-3} m s^{-1} remains close to 0.918 km throughout the parameter sweep, whereas a central region with $V \geq 10^{-2}$ m s^{-1} appears only when the constitutive response time is finite and expands to approximately 0.449 km. The broader footprint is therefore controlled mainly by the imposed stress perturbation and distributed elastic coupling, while the faster inner core is strongly controlled by constitutive memory. This distinction cannot be inferred from peak velocity alone. Two nucleation episodes with similar overall dimensions may have substantially different internal velocity distributions and may consequently interact differently with neighboring fault segments, geometric discontinuities, or velocity-strengthening barriers. The spatially resolved identification of a comparatively stable outer nucleation footprint and a delay-sensitive inner high-velocity core is, in our view, the most important new scientific contribution of the paper.

https://doi.org/10.5194/egusphere-2026-4365
Preprint. Discussion started: 24 July 2026

The increase in peak velocity can be understood as a transient mismatch between the current sliding state and the delayed state-evolution feedback. During acceleration, the friction law evaluates healing and state consumption using an earlier, slower configuration. The state variable therefore does not adjust at the rate prescribed by the instantaneous slip velocity, allowing a larger velocity excursion before the feedback catches up. Because stress is redistributed between neighboring points, this mismatch is not spatially uniform. It is strongest near the center of the imposed perturbation, where acceleration is largest, and it progressively modifies the shoulders of the velocity profile. The profiles in Figure 3 and the center-point histories in Figure 4 consequently show more than simple amplification: they reveal a delay-dependent change in the trajectory by which the system approaches its maximum response.

The local crossing of 10^{-2} m s^{-1} is also physically informative. It shows that the constitutive delay can move a nucleation process from sub-threshold acceleration to locally dynamic slip speeds without changing the imposed stress perturbation. Figure 7 further shows that velocity-threshold crossing and spatial propagation are separate diagnostics. In the investigated Master configuration, the higher velocities remain confined to the nucleation-scale region. This outcome is useful rather than incidental, because it isolates a pre-propagation stage at which constitutive memory already has a strong measurable effect. It suggests that the onset of locally rapid slip and the subsequent recruitment of the surrounding fault should be treated as related but distinct transitions. A fully dynamic model can subsequently test whether the larger and wider high-velocity core produced by finite t_c changes the conditions required for that second transition.

The dimensionless quantity $\Pi_d = t_c V_{max}/D_c$ provides a compact way to express the strength of the observed memory effect. It compares the imposed response time with the characteristic state-evolution time D_c/V_{max}. The monotonic increase of normalized peak velocity and high-velocity extent with Π_d indicates that the influence of delay becomes significant when the fault can slip through an appreciable fraction of D_c before the state feedback has fully adapted. This interpretation links the new parameter t_c to the established rate-and-state length D_c and makes comparisons between simulations with different characteristic distances more transparent. Because V_{max} is an output, Π_d is presently a diagnostic rather than a fully predictive control parameter. A broader parameter study should examine whether V_{max} can be replaced by an initial, reference, or onset velocity to obtain an input-based scaling law.

The results also complement microphysical and multi-mechanism friction models. Ikari et al. (2016) and van den Ende et al. (2018) related rate-and-state behavior to gouge-scale deformation and contact processes, while Barbot (2022) considered competing healing mechanisms with rate, state, and temperature dependence. Such formulations enrich the physical content of friction but generally do so by adding mechanisms or state dependencies. The approach used here is deliberately minimal: it asks whether a finite response time, without introducing a new weakening mechanism or recalibrating the steady-state friction curve, can change nucleation. The affirmative result indicates that constitutive timescale should be treated alongside constitutive strength. This provides a parsimonious route for representing unresolved contact reorganization, gouge rearrangement, or delayed healing, while leaving the precise microphysical origin of t_c to laboratory calibration.

From a modelling perspective, the novelty is therefore threefold. First, an explicit local delayed ageing law is embedded in a spatially distributed earthquake-nucleation model, bridging earlier low-dimensional delay systems and continuum rate-and-state nucleation studies. Second, the study quantifies the effect of t_c using mutually complementary temporal and spatial observables—peak velocity, center-point histories, velocity profiles, threshold extents, and a moment proxy—rather than classifying the response only by a single time series. Third, it identifies Π_d and the two-scale spatial response as practical diagnostics for subsequent model comparison. Taken together, these elements show that temporal organization is a constitutive modelling dimension in its own right. The significant effect is not merely that the delayed model evolves later, but that it follows a different nucleation path and produces a different spatially organized state at the same physical time.

Several limitations define the scope of this contribution. The calculations use one Master parameter configuration, a reduced-order one-dimensional elastic closure, periodic boundaries, and a prescribed nucleation perturbation. The values of H and η are model closures rather than independently measured fault properties, and the explored interval of t_c has not yet been calibrated against laboratory velocity-step or slide–hold–slide experiments. It is therefore premature to assign a universal value of t_c to natural faults or to infer earthquake-scale source properties from the present simulations. The next tests should vary D_c, effective normal stress, the velocity-weakening patch size, transition width, and perturbation amplitude; perform grid and closure sensitivity analyses; and implement the same delayed law in a fully dynamic continuum solver. Experimental work should determine whether transient friction data

https://doi.org/10.5194/egusphere-2026-4365
Preprint. Discussion started: 24 July 2026

support a resolvable lag between velocity change and state adjustment and whether that lag remains constant or depends on slip history, temperature, gouge thickness, or effective stress.

Within these limits, the principal contribution is clear: the paper demonstrates, in a controlled spatial model, that finite-time state adaptation can amplify nucleation and reorganize its internal spatial structure independently of the conventional rate-and-state parameters. Existing RSF nucleation studies establish the importance of state-law choice, and earlier delayed block models establish the possibility of frictional memory; the present work connects these two lines of research. By showing that a stable outer nucleation footprint can coexist with a delay-sensitive high-velocity core, it introduces a spatial signature of friction memory that can be sought in more complete simulations and, eventually, in laboratory or geophysical observations. This spatially resolved constitutive signature—not a claim of unrestricted rupture propagation—is the strongest scientific advance supported by Figures 1–7.

5. Conclusions

This study examined how a finite constitutive response time modifies earthquake nucleation in a spatially distributed fault model governed by rate-and-state friction. The delayed formulation preserves the conventional friction parameters and steady-state structure of the ageing law, but allows state evolution to respond to velocity after a finite interval t_c. This controlled construction makes it possible to distinguish the influence of temporal constitutive organization from the effects of elastic properties, fault geometry, initial stress, nucleation perturbation, and the standard rate-and-state parameters. For the common Master configuration used in Figures 1–7, constitutive delay produces a systematic and physically coherent amplification of the nucleation response.

Increasing t_c from 0 to 0.12 s raises the maximum slip velocity from 7.38×10^{-3} to 1.38×10^{-2} m s^{-1}, corresponding to an increase of approximately 87%. The effect is not restricted to peak amplitude. Delayed state evolution changes the timing of acceleration, sharpens the central velocity maximum, modifies the profile shoulders, and permits local crossing of the adopted dynamic-velocity threshold of 10^{-2} m s^{-1}. The results therefore show that frictional memory changes the path by which nucleation develops, rather than simply shifting an otherwise identical response in time.

The principal scientific contribution is the identification of two spatial scales with different sensitivities to constitutive memory. The broader region exceeding 10^{-3} m s^{-1} remains approximately 0.918 km wide throughout the tested range and is primarily associated with the prescribed nucleation perturbation and distributed elastic coupling. In contrast, the inner region exceeding 10^{-2} m s^{-1} emerges only for finite response times and expands to approximately 0.449 km. A stable outer nucleation footprint can therefore coexist with a strongly delay-sensitive high-velocity core. This spatial signature extends earlier delayed one- and two-block earthquake models by demonstrating how frictional memory is expressed within a distributed nucleation zone. It also complements classical continuum rate-and-state studies, which have primarily investigated the choice of state law under the assumption of instantaneous constitutive response.

The dimensionless diagnostic $\Pi_d = t_c V_{max}/D_c$ provides a concise measure of the relative importance of delayed adaptation. Its relationship with normalized peak velocity and high-velocity extent indicates that memory becomes influential when appreciable slip can accumulate relative to D_c before the state feedback has adjusted. Although Π_d is presently an output-based diagnostic, it offers a useful basis for comparing simulations with different values of t_c and D_c and for developing a more general scaling description of delayed-state nucleation.

The next stage of research should first establish the robustness of these findings across a multidimensional parameter space. Systematic simulations should vary t_c together with D_c, effective normal stress, the velocity-weakening contrast $b - a$, nucleation-zone size, transition width, initial stress, and perturbation amplitude. This analysis should determine whether the two-scale spatial response persists, identify the combinations that control the onset and width of the high-velocity core, and test whether Π_d can be reformulated using an input velocity so that it becomes predictive rather than diagnostic. Grid-refinement tests and sensitivity analyses for the reduced-order closure parameters H and η should accompany this sweep.

A second priority is implementation of the same delayed-state law in a fully dynamic continuum framework, such as a validated spectral boundary-integral, finite-element, or discontinuous-Galerkin solver. That extension should retain the Master configuration and compare instantaneous and delayed cases using rupture length, rupture-front speed, stress drop, radiated energy, seismic moment, and arrest position. The key question for that stage is whether the larger delay-sensitive high-velocity core identified here changes the transition from localized nucleation to self-sustained

14

dynamic propagation when wave-mediated stress transfer is resolved explicitly. The present results provide both the constitutive formulation and the quantitative benchmarks required for such verification.

Finally, laboratory calibration is required to connect t_c with measurable fault-zone processes. Velocity-step and slide–hold–slide experiments should be analysed for a resolvable lag between an imposed velocity change and the corresponding state or friction adjustment. Tests conducted over different effective normal stresses, gouge thicknesses, temperatures, and accumulated slips could determine whether t_c is approximately constant or evolves with fault condition and loading history. Combining these experiments with the proposed dynamic simulations would allow frictional memory to progress from a phenomenological delay parameter to a physically calibrated constitutive timescale.

Within the scope of the present model, the central conclusion is that finite-time state adaptation is a consequential component of earthquake nucleation. It modifies both the intensity and spatial organization of accelerated slip independently of the conventional rate-and-state parameters. By linking explicit frictional delay to a spatially resolved nucleation signature, this study provides a reproducible starting point for testing how constitutive memory may influence the subsequent transition to dynamic earthquake rupture.

Code and data availability

The model code, configuration files, processed metrics, and figure-generation scripts are provided as a review asset accompanying this submission. Before final publication, the complete reproducibility package and underlying simulation outputs will be deposited in Zenodo under a CC BY 4.0 or compatible open licence, and the resulting DOI will replace this provisional statement.

Supplement link

The Supplement contains the Master parameter table, numerical classifications, and additional reproducibility information.

Author contributions

SK and NV wrote the manuscript. NV performed the calculations and numerical analysis. SK prepared the final version of the manuscript. Both authors reviewed and approved the submitted version.

Competing interests

The authors declare that they have no conflict of interest.

Acknowledgements

The authors acknowledge the institutional support of the Jaroslav Černi Water Institute, the Faculty of Technical Sciences of the University of Novi Sad, and the University of Belgrade – Faculty of Mining and Geology.

Financial support

This research received no external funding.

References

Ampuero, J.-P., & Ben-Zion, Y. (2008). Cracks, pulses and macroscopic asymmetry of dynamic rupture on a bimaterial interface with velocity-weakening friction. *Geophysical Journal International*, *173*(2), 674–692. doi:10.1111/j.1365-246X.2008.03736.x

Ampuero, J.-P., & Rubin, A. M. (2008). Earthquake nucleation on rate and state faults—Aging and slip laws. *Journal of Geophysical Research: Solid Earth*, *113*, B01302. doi:10.1029/2007JB005082

Andrews, D. J. (1976). Rupture propagation with finite stress in antiplane strain. *Journal of Geophysical Research*, *81*(20), 3575–3582. doi:10.1029/JB081i020p03575

15

Andrews, D. J. (2005). Rupture dynamics with energy loss outside the slip zone. *Journal of Geophysical Research: Solid Earth, 110*, B01307. doi:10.1029/2004JB003191

Barbot, S. (2022). A rate-, state-, and temperature-dependent friction law with competing healing mechanisms. *Journal of Geophysical Research: Solid Earth, 127*(11), e2022JB025106. doi:10.1029/2022JB025106

Ben-Zion, Y. (2008). Collective behavior of earthquakes and faults: Continuum–discrete transitions, progressive evolutionary changes, and different dynamic regimes. *Reviews of Geophysics, 46*, RG4006. doi:10.1029/2008RG000260

Burridge, R., & Knopoff, L. (1967). Model and theoretical seismicity. *Bulletin of the Seismological Society of America, 57*(3), 341–371.

Carlson, J. M. (1991). A two-dimensional model of a fault. *Physical Review A, 44*(9), 6226–6232. doi:10.1103/PhysRevA.44.6226

Carlson, J. M., & Langer, J. S. (1989). Mechanical model of an earthquake fault. *Physical Review A, 40*(11), 6470–6484. doi:10.1103/PhysRevA.40.6470

Dieterich, J. H. (1979). Modeling of rock friction: 1. Experimental results and constitutive equations. *Journal of Geophysical Research, 84*(B5), 2161–2168. doi:10.1029/JB084iB05p02161

Dieterich, J. H., & Kilgore, B. D. (1994). Direct observation of frictional contacts: New insights for state-dependent properties. *Pure and Applied Geophysics, 143*, 283–302. doi:10.1007/BF00874332

Dunham, E. M., Belanger, D., Cong, L., & Kozdon, J. E. (2011). Earthquake ruptures with strongly rate-weakening friction and off-fault plasticity, Part 1: Planar faults. *Bulletin of the Seismological Society of America, 101*(5), 2296–2307. doi:10.1785/0120100075

Erickson, B. A., Dunham, E. M., & Khosravifar, A. (2017). A finite difference method for off-fault plasticity throughout the earthquake cycle. *Journal of the Mechanics and Physics of Solids, 109*, 50–77. doi:10.1016/j.jmps.2017.08.002

Frank, W. B., & Brodsky, E. E. (2019). Daily measurement of slow slip from low-frequency earthquakes is consistent with ordinary earthquake scaling. *Science Advances, 5*(10), eaaw9386. doi:10.1126/sciadv.aaw9386

Goldsby, D. L., & Tullis, T. E. (2011). Flash heating leads to low frictional strength of crustal rocks at earthquake slip rates. *Science, 334*(6053), 216–218. doi:10.1126/science.1207902

Heaton, T. H. (1990). Evidence for and implications of self-healing pulses of slip in earthquake rupture. *Physics of the Earth and Planetary Interiors, 64*(1), 1–20. doi:10.1016/0031-9201(90)90002-F

Ikari, M. J., Carpenter, B. M., & Marone, C. (2016). A microphysical interpretation of rate- and state-dependent friction for fault gouge. *Geochemistry, Geophysics, Geosystems, 17*(5), 1660–1677. doi:10.1002/2016GC006286

Kame, N., Fujita, S., Nakatani, M., & Kusakabe, T. (2015). Earthquake nucleation on faults with a revised rate- and state-dependent friction law. *Pure and Applied Geophysics, 172*(8), 2237–2246. doi:10.1007/s00024-013-0744-0

Kaneko, Y., Lapusta, N., & Ampuero, J.-P. (2008). Spectral element modeling of spontaneous earthquake rupture on rate and state faults: Effect of velocity-strengthening friction at shallow depths. *Journal of Geophysical Research: Solid Earth, 113*, B09317. doi:10.1029/2007JB005553

Kostić, S., Franović, I., Todorović, K., & Vasović, N. (2013a). Friction memory effect in complex dynamics of earthquake model. *Nonlinear Dynamics, 73*, 1933–1943. doi:10.1007/s11071-013-0914-8

Kostić, S., Vasović, N., Franović, I., & Todorović, K. (2013b). Dynamics of simple earthquake model with time delay and variation of friction strength. *Nonlinear Processes in Geophysics, 20*, 857–865. doi:10.5194/npg-20-857-2013

Lapusta, N., Rice, J. R., Ben-Zion, Y., & Zheng, G. (2000). Elastodynamic analysis for slow tectonic loading with spontaneous rupture episodes on faults with rate- and state-dependent friction. *Journal of Geophysical Research: Solid Earth, 105*(B10), 23,765–23,789. doi:10.1029/2000JB900250

Marone, C. (1998). Laboratory-derived friction laws and their application to seismic faulting. *Annual Review of Earth and Planetary Sciences, 26*, 643–696. doi:10.1146/annurev.earth.26.1.643

Nishikawa, T., Matsuzawa, T., Ohta, K., Uchida, N., Nishimura, T., & Ide, S. (2019). The slow earthquake spectrum in the Japan Trench illuminated by the S-net seafloor observatories. *Science, 365*(6455), 808–813. doi:10.1126/science.aax5618

Obara, K., & Kato, A. (2016). Connecting slow earthquakes to huge earthquakes. *Science, 353*(6296), 253–257. doi:10.1126/science.aaf1512

Passarelli, L., Selvadurai, P. A., Rivalta, E., & Jónsson, S. (2021). The source scaling and seismic productivity of slow slip transients. *Science Advances, 7*(32), eabg9718. doi:10.1126/sciadv.abg9718

Rice, J. R. (1993). Spatio-temporal complexity of slip on a fault. *Journal of Geophysical Research: Solid Earth, 98*(B6), 9885–9907. doi:10.1029/93JB00191

Rice, J. R. (2006). Heating and weakening of faults during earthquake slip. *Journal of Geophysical Research: Solid Earth, 111*, B05311. doi:10.1029/2005JB004006

Rubin, A. M., & Ampuero, J.-P. (2005). Earthquake nucleation on (aging) rate and state faults. *Journal of Geophysical Research: Solid Earth, 110*, B11312. doi:10.1029/2005JB003686

Ruina, A. (1983). Slip instability and state variable friction laws. *Journal of Geophysical Research: Solid Earth, 88*(B12), 10,359–10,370. doi:10.1029/JB088iB12p10359

Tan, Y. J., & Marsan, D. (2020). Connecting a broad spectrum of transient slip on the San Andreas Fault. *Science Advances*, *6*(33), eabb2489. doi:10.1126/sciadv.abb2489

van den Ende, M. P. A., Chen, J., Ampuero, J.-P., & Niemeijer, A. R. (2018). A comparison between rate-and-state friction and microphysical models, based on numerical simulations of fault slip. *Tectonophysics, 733*, 273–295. doi:10.1016/j.tecto.2017.11.040

Vasović, N., Kostić, S., Franović, I., & Todorović, K. (2016). Earthquake nucleation in a stochastic fault model of globally coupled units with interaction delays. *Communications in Nonlinear Science and Numerical Simulation, 38*, 117–129. doi:10.1016/j.cnsns.2016.02.011

Viesca, R. C. (2023). Frictional state evolution laws and the non-linear nucleation of dynamic shear rupture. *Journal of the Mechanics and Physics of Solids, 173*, 105221. doi:10.1016/j.jmps.2023.105221

Wollherr, S., Gabriel, A.-A., & Uphoff, C. (2018). Off-fault plasticity in three-dimensional dynamic rupture simulations using a modal Discontinuous Galerkin method on unstructured meshes: Implementation, verification and application. *Geophysical Journal International, 214*(3), 1556–1584. doi:10.1093/gji/ggy213